A unique No-Go Decay cleavage in mRNA exit-tunnel of ribosome produces 5'-OH ends phosphorylated by Rlg1

Albertas Navickas[1#•], Sébastien Chamois[1#], Rénette Saint-Fort[1], Julien Henri[1], Claire Torchet[1,] and Lionel Benard[1]*

[1]Institut de Biologie Physico-Chimique, UMR8226, CNRS, Sorbonne Université, Paris, France

[#]Co-first authors

***Correspondence to** Lionel BENARD, e-mail address: lionel.benard@ibpc.fr

[•]present address: Department of Biochemistry and Biophysics
University of California, San Francisco
San Francisco, CA 94158, USA

Keywords:

No-Go Decay, mRNA surveillance, Endoribonuclease, RNA kinase, 5'-hydroxyl RNA, Rlg1, Exoribonuclease, Xrn1, Dxo1, disome, Ribosomal mRNA exit tunnel

ABSTRACT

The No-Go Decay (NGD) mRNA surveillance pathway degrades mRNAs containing stalled ribosomes. An endoribonuclease has been proposed to initiate cleavages upstream of the stall sequence. However, primary site of cleavage remains unknown. Indeed, direct evidence that two RNA fragments resulting from a precise and unique cleavage has never been obtained. We used mRNAs expressing a 3'-ribozyme to produce truncated transcripts *in vivo* that mimic naturally occurring truncated mRNAs, known to trigger NGD. We analysed ribosome associated NGD cleavage products at single-nucleotide resolution and show that a precise endonucleolytic cleavage event occurs within the mRNA exit tunnel of the ribosome, 8 nucleotides upstream of the first P-site residue. The first two stalled ribosomes are apparently not competent for mRNA cleavage. We demonstrate that NGD cleavage within the third or upstream ribosomes produces 5'-hydroxylated RNA fragments that are phosphorylated by the Rlg1/Trl1 kinase. The resulting 5'-phosphorylated RNA fragments are digested by the 5'-3 exoribonuclease Xrn1, but surprisingly, can also be trimmed by the 5'-3' exoribonuclease activity of Dxo1 in Xrn1 deficient cells.

INTRODUCTION

The No-Go Decay (NGD) mRNA surveillance pathway degrades mRNAs containing stalled ribosomes [1,2]. NGD occurs when translation elongation is blocked by the presence of stable intra- or intermolecular RNA structures, enzymatic cleavage, chemically damaged sequences, rare codons or mRNA depurination [1,3-8]. This mRNA degradation process is dependent on translation and involves an unidentified endoribonuclease that cleaves just upstream of the stall sequence [1,5,6,9]. Other mRNA surveillance pathways can also ultimately lead to NGD. For instance, transcripts synthesized without a stop codon due to premature polyadenylation have stalled ribosomes that are initially detected by the Non-stop decay (NSD) decay pathway [9,10]. NSD targeted mRNAs are cleaved by an uncharacterized mechanism and become targets of NGD when ribosomes reach the new 3'-end and stall [9,11 ,12]. NGD thus plays a key role in resolving translational issues potentially detrimental to cellular homeostasis. When mRNAs are truncated, the stalled ribosomes are rescued in a process mediated by the Dom34/Hbs1 complex that dissociates the ribosomal subunits [5]. Their association with the 60S subunit is recognized by the Ribosome Quality Control (RQC) pathway leading to the rapid degradation of the nascent peptide [13-15]. However, despite extensive study, the precise location of NGD cleavage and the mechanism of degradation of the resulting RNA fragment remain unknown.

In this paper, we focused on the fate of NGD-cleaved mRNAs, with an initial goal of mapping the sites of mRNA cleavage with accuracy. Two major obstacles to achieving this objective are that NGD fragments are rapidly attacked by 5'-3' and 3'-5' exoribonucleases after ribosome dissociation [5] and that simultaneously blocking the 5'-3' and 3'-5' exoribonuclease decay pathways is synthetic lethal [16]. It has been shown, however, that the stability of such mRNAs is largely dependent on the Dom34/Hbs1 complex [5,17]. In *dom34* mutant cells, ribosomes stalled at the 3'-end of truncated mRNAs inhibit the degradation by the exosome and facilitate the detection of sequential endonucleolytic cleavages upstream of the ribosomal stall site [5]. Interestingly, *dom34* and *xrn1* mutations (inactivating the main 5'-3' exonucleolytic degradation pathway) are not synthetic lethal [1]. Moreover, NGD endonucleolytic cleavages still occur in the absence of Dom34 [2,3]. The limited 3'-5' degradation of specific mRNA targets (in the absence of Dom34) combined with 5'-3' exoribonuclease mutants thus allows an accumulation of RNA fragments resulting from endonucleolytic cleavages whose extremities can be mapped accurately. We created a series

of truncated mRNAs *in vivo* by insertion of a hammerhead ribozyme sequence (Rz), known to generate NGD targeted mRNAs [5]. These constructions mimic chemically or enzymatically cleaved mRNAs, or those resulting from abortively spliced mRNAs that are processed by the NGD pathway [5,9,18]. As anticipated, these designed truncated 3'-ends block ribosomes at determined positions and, because ribosomes guide NGD mRNA cleavages [5,19], we were able to detect 3'-NGD RNA fragments of specific sizes. By analysing these RNAs in detail, we demonstrated the existence of a unique cleavage site 8 nucleotides (nts) upstream of the first P-site nt and therefore propose that this event occurs within the mRNA exit tunnel of the ribosome. We show that the 3'-NGD cleavage products have a hydroxylated 5'-extremity and are then phosphorylated by the RNA kinase activity of the tRNA ligase Rlg1/Trl1 to allow degradation by the 5'-3' exoribonuclease Xrn1. In the absence of Xrn1, the alternative 5'-3' exoribonuclease Dxo1 takes over.

RESULTS

Mapping the 5'-ends of 3'-NGD RNA fragments at single-nucleotide resolution

To generate 3'-truncated mRNA substrates for NGD *in vivo*, we inserted a hammerhead ribozyme sequence [20] in the 3'-sequence of *URA3* gene ORF (mRNA1Rz). This results in the production of an mRNA that lacks a stop codon and a polyadenylated tail, called mRNA1 in Fig. 1a and Supplementary Fig. 1a, and known to be an NGD target [5]. We first verified that we could detect NGD cleavages in the 3'-proximal region of mRNA1, by northern blotting with a probe corresponding to the 3'-end (probe prA, Fig. 1a and Supplementary Fig. 1a). The upstream and downstream cleavage products are referred to as 5'-NGD and 3'-NGD RNAs, respectively (Fig. 1a). We indeed detected a ladder of 3'-NGD RNA fragments in *dom34* mutant cells (Fig. 1b), in the presence or absence of active 5'-3' or 3'-5' exonucleolytic decay pathways, *i.e. xrn1* or *ski2* mutations, respectively [21]. In agreement with the current NGD model in which endonucleolytically cleaved 3'-NGD fragments are primarily degraded by the 5'-3' exoribonuclease Xrn1 [5], inactivation of the 5'-3' RNA decay pathway (*xrn1* mutant cells) produced a different ladder of 3'-NGD RNAs compared to WT or the *ski2* mutant. This was confirmed by a higher resolution PAGE analysis followed by northern blotting (Fig. 1c). The PAGE analysis was completed by mapping the 5'-ends of the 3'-NGD RNA fragments in the *dom34* and *dom34*/*xrn1* mutants by primer extension experiments with prA (Fig. 1d). We showed that the truncated mRNAs produce several discrete 3'-NGD RNA bands (B1-5) that can be mapped to single-nucleotide resolution. B5 (77 nts) and the major RNA species B1 (47 nts) were only detected in the presence of active 5'-3' exoribonuclease Xrn1 (Fig. 1b, 1c and 1d); B3 (68 nts) and B2 (65 nts) RNAs were exclusively observed in the *xrn1* mutant cells, and B4 (71 nts) was detected in all three strains. The sizes of the major B1 and B5 RNAs differ by 30 nts (Fig. 1d), consistent with the length of mRNA covered by an individual ribosome [22]. We therefore surmised that the difference in size is most likely due to the presence of an extra ribosome protecting the B5 RNA species from 5'-3' degradation by Xrn1 [23], compared to B1. This prompted us to analyse how these 3'-NGD RNAs are protected by ribosomes *in vitro*.

Ribosome protection of 3'-NGD RNA fragments from RNase activity

To assess the protection of 3'-NGD RNAs by ribosomes, we first performed an Xrn1 protection assay (Fig. 1e). We focused on the fate of the major RNA species B1 (47 nts) and B5 (77 nts) detected in *dom34* cell extracts that likely correspond to RNAs protected from Xrn1 digestion *in vivo* by trisomes and disomes, respectively. Indeed, an association of a 47-nt RNA species with disomes was deduced from ribosome profiling experiments [9,19,22-24] and is explained by the approximate size of the trailing ribosome protecting a full ribosome footprint (28–30 nt) and the leading ribosome protecting a half footprint to the site of mRNA truncation (16–17 nts with no RNA or an incomplete codon in the A-site). An additional ribosome would thus be expected to protect a ~77-nt RNA. We thus verified that Xrn1 treatment of RNA present in *dom34* cell extracts had no impact on B5 and B1 RNAs *in vitro* (Fig. 1e), since we anticipated that these RNAs were already protected from Xrn1 digestion by ribosomes *in vivo*, and thus should be still protected in cell extracts *in vitro*. Interestingly, the persistence of B4 RNA after Xrn1 treatment suggests that this RNA is also potentially protected by ribosomes in the *dom34* background (Fig. 1e). We also added purified Xrn1 to cell extracts of the *dom34*/*xrn1* strain *in vitro* and showed that it can efficiently recapitulate the production of the B1 species observed in Xrn1-containing cells *in vivo*. The appearance of the B1 RNA was inversely correlated to the amount of B4, B3 and B2 RNAs remaining, suggesting that these three species have unprotected 5'-protruding RNA extremities *in vivo,* due to the absence of the 5'-3' exoribonuclease Xrn1 (Fig. 1e). The B5 RNA was also generated at the expense of some larger species by Xrn1 treatment *in vitro*, consistent with the presence of trisomes on this species in the *dom34*/*xrn1* cell extracts (Fig. 1e). Based on these experiments, we propose that B1 (47 nts) and B5 RNAs (77 nts) correspond to Xrn1-trimmed RNAs protected by two and three ribosomes, respectively [23] and that the 71 nt Bd4 RNA is also protected from Xrn1 by three ribosomes.

To validate the presence and number of ribosomes on 3'-NGD RNAs by a second method, and particularly the presence of trisomes on the 71-nt B4 RNA, we also performed RNase I protection assays on cell extracts of *dom34* and *dom34 xrn1Δ* strains. We hypothetised that the B5 and B4 RNAs protected from RNase I by three ribosomes should be detectable with both probes prA and prD (Fig. 1f). The presence of two or three ribosomes on the major RNA species B1, B4 and B5 in *dom34* cells (deduced from primer extension experiments and Xrn1 treatment *in vitro*) would preferentially conduct RNase I to cleave at three major sites, Cut1, 2 and 3 in Fig. 1f. After RNase I treatment (Fig. 1g), the accumulation

of RNase I protected RNAs of similar size to B5 suggested that this RNA is covered by trisomes in *dom34* (Fig. 1g). It is known that RNase I and Xrn1 cleave about 15 nts [9] and 17 nts [23] upstream of the first nt of the ribosomal A-site, respectively. We thus expected 5'-end of the B5 RNA to be 2 nt shorter after RNase I treatment compared to Xrn1, if we had accurately surmised the positions of ribosomes on this RNA. Indeed, primer extension experiments confirmed that ribosomes protect 75-nt RNAs against RNase I in the *dom34* background (Supplementary Fig. 1b and Supplementary Fig. 1c). The equivalent of the B1 RNA was 45-46 nt in size after RNase I treatment (Supplementary Fig. 1d) and, surprisingly, the B4 RNA was not detected using probe prA (Fig. 1g). We thus wondered whether RNase I cleaved preferentially at Cut3 (Fig. 1f), thus preventing the detection of B4 using probe prA. We probed the membrane in Fig. 1g with prD (Fig. 1h), and two distinct RNA species were detected, corresponding to B5 and B4 processed by RNase I, and inefficiently cleaved at the Cut2 site (Fig. 1f). We thus proposed that the 5'-extremities of B4 RNA are protected by ribosomes. We conducted the same experiment on the B4 RNA from *xrn1/dom34* cell extracts. These RNAs were sensitive to Xrn1 treatment *in vitro* (Fig. 1e), and using probe prD to detect the B4 RNA specifically, we observed that these RNAs were also protected from RNase I to a similar extent as B4 in *dom34* cell extracts (Fig. 1h). Together these results allow us to infer the precise positions of ribosomes on RNA species in the different mutant backgrounds (Fig. 1i). In the *dom34* context, the B1 and B5 RNAs correspond to RNAs covered by disomes and trisomes, respectively, after processing by Xrn1 *in vivo* (Fig. 1i). We propose that three ribosomes cover the 71-nt B4 RNA in *dom34* mutant cell extracts as this species is resistant to Xrn1 (Fig. 1e) and its 5'-region is protected from RNase I digestion *in vitro* (Fig. 1h). Whether two or three ribosomes dwell on the 71-nt Bd4 RNA in *xrn1/dom34* mutant cell extracts is unclear as this species is sensitive to Xrn1 *in vitro* (*i.e.* have 5'-ribosome-free extensions that can be pared down to B1 by Xrn1 digestions) (Fig. 1e), which would be consistent with protection by two ribosomes, but resistant to RNase I (Fig. 1h), more consistent with three.

The heterogeneity of 3'-NGD RNA fragments in Xrn1 deficient cells is produced by Dxo1

We thus strongly suspected that B4 RNAs were original NGD products, and because they were exclusively detected in Xrn1 deficient cells, we speculated that the B3 and B2 RNAs might be derived from B4 RNAs by an alternative 5'-3' exoribonuclease. We therefore asked whether the 5'-3' exoribonucleolytic activity of Dxo1, on the margins of its important role in 5'-end capping quality control [25], might explain the presence of the B3 and B2 RNAs. Remarkably, deletion of both *xrn1* and *dxo1* genes in a *dom34* background completely abolished the production of the B3 and B2 RNAs, and only the B4 3'-NGD species remained detectable by northern blot analysis (Fig. 2a) or in primer extension assays (Supplementary Fig. 2a). Complementation of the *dom34*/*xrn1*/*dxo1* mutant with wild-type Dxo1 restored B3 and B2 RNA production to a significant extent, but a catalytic mutant failed to do so (Fig. 2b). We took advantage of the almost exclusive presence of the B4 3'-NGD RNAs in *dom34*/*xrn1*/*dxo1* mutant cells to re-question how this RNA is protected by ribosomes, by adding Xrn1 to cell extracts as described above. Some of the B4 RNA was Xrn1-resistant (Supplementary Fig. 2b) in accordance with our hypothesis that a portion of this species is still protected by three ribosomes in *xrn1*/*dom34* cell extracts (Supplementary Fig. 1c). Remarkably, most of the B4 RNA was also degraded to a 47-nt species (Supplementary Fig. 2b), strongly suggesting that disomes persist on the majority of the 3'-end of truncated RNAs in *dom34*/*xrn1*/*dxo1* cells *in vivo*. We thus conclude that two populations of B4 RNAs co-exist *in vivo* in Xrn1 deficient cells, with one resembling B4 RNAs covered by three ribosomes like in *dom34* mutants and the other having 5'-protuding RNA extremities due to the absence of 5'-3' exoribonucleases.

We performed a number of experiments to probe the role of Dxo1 under conditions where Xrn1 is still present, but when its activity is attenuated. Inhibition of the 5'-3' exoribonuclease activity of Xrn1 occurs upon accumulation of the metabolite 3'-phospho-adenosine-5'-phosphate (pAp), for example in Met22 deficient cells, or in cells exposed to high levels of toxic ions such as sodium or lithium [26,27]. Remarkably, in cells containing Xrn1, the *met22* mutation or the addition of lithium led to the accumulation of B3 and B2 RNAs, while still maintaining the production of the B5 and B1 species (Fig. 2c and Supplementary Fig. 2c). Hence, Dxo1 can participate in 3'-NGD RNA trimming even under conditions where Xrn1 is still partially active.

We asked whether Dxo1 trimming of NGD-cleaved mRNAs is dependent on the nature of the nucleotide sequence. To do this, we modified the nucleotide sequence encompassing the site of the potential endonucleolytic cleavage by building derivatives of mRNA1 (called mRNA2, 3 and 4). We probed the resulting decay intermediates in *dom34*, *dom34*/*xrn1* and *dom34*/*xrn1*/*dxo1* mutants, and observed that although the B2 and B3 3'-NGD RNA intermediates produced by Dxo1 from these RNAs were slightly different in levels and in size compared to their equivalents from mRNA1, the production of the B4 RNA was remarkably preserved in all four constructs (Fig. 2d and Supplementary Fig. 2d). Taken together, these results provide evidence that B2 and B3 RNAs are products of Dxo1 activity and that Dxo1 plays a general role in supporting Xrn1 in the degradation of the B4 3'-NGD RNA.

Identification of the primary NGD endonucleolytic cleavage site

The results described above suggested that the B4 RNA is the major 3'-product of NGD cleavage in our constructs and that it is trimmed to smaller sizes by Xrn1 and Dxo1. While its resistance to Xrn1 *in vitro* (Fig. 1e) could be explained by a third ribosome dwelling after cleavage, we also considered the possibility that its 5'-phosphorylation state could contribute to its stability, since both Xrn1 and Dxo1 require 5'-phosphorylated extremities to degrade RNA [25,28]. We therefore asked whether the B4 RNA naturally has a monophosphate or a hydroxyl group at its 5'-end by treating RNA purified from *dom34* cell extracts with T4 polynucleotide kinase to see whether this would stimulate attack of B4 by Xrn1 *in vitro*. Remarkably, the B4 RNA was completely degraded by Xrn1 after 5'-phosphorylation by T4 kinase *in vitro* (Fig. 3a), demonstrating that the B4 RNA has a 5'-OH extremity in *dom34* cells. 5'-hydroxyl and 2'-3' cyclic phosphate 3' extremities are typically generated by metal-independent endoribonucleolytic reactions [29].

By definition endonucleolytically cleaved NGD mRNAs result in 5' and 3'-NGD RNA fragments. We thus searched for the corresponding 5'-NGD fragment for the B4 3'-NGD RNA. To map the 3'-end of 5'-NGD RNAs, total RNA preparations from *ski2* and *ski2*/*dom34* mutants were ligated to a pre-adenylated oligonucleotide linker using truncated RNA ligase (Fig. 3b) [30]. The *ski2* mutant context was used to limit 3'-trimming of these RNAs *in vivo*. RNAs were pre-treated with T4 polynucleotide kinase to modify 2'-3' cyclic phosphates to 3'-OH to permit RNA ligation [30]. Linker-ligated RNAs were reverse transcribed, amplified by PCR and cloned for sequencing, using a method called 3'-RNA

ligase mediated RACE (called 3'-RACE below) (Fig. 3b) [31]. The major RT-PCR product was of the expected size (66 bp; Fig. 3c and Supplementary Fig. 3a) and verified by sequencing resulting clones (Fig. 3d). The identification of a matching 5'-NGD fragment for the B4 3'-NGD RNA, confirms that an endonucleolytic event occurred at this precise position. Remarkably, the same procedure performed on RNAs isolated from *ski2* mutants where Dom34 is still active yielded the same major PCR product, also verified by sequence (Supplementary Fig. 3b).

The fate of 5'-NGD RNAs

We anticipated that following NGD cleavage of mRNA1, ribosomes that had initiated translation on the 5'-NGD fragments would advance to the new 3'-end and the RNA subjected to Xrn1 trimming, similar to the process that generates B1 and B5 (Fig. 4a). Since the B4 3'-NGD RNAs are cut in the +1 reading frame (Fig. 1i), upstream ribosomes on these 5'-NGD RNAs would be expected to stall with one nucleotide in ribosome A-site (Fig. 4a and Supplementary Fig. 4) and as result produce new RNA fragments 47+1, 77+1 nts, protected by two or three ribosomes, respectively (see Supplementary Fig. 4). Indeed, using probe prG, complementary to the new 3'-ends generated by NGD cleavage, we detected RNA fragments consistent with a 1-nt increase in size compared to prA by northern blotting the same membrane (Fig. 4b). We mapped the 5'-ends of these new ribosome protected fragments by primer extension assays using prG (Fig. 4c and Supplementary Fig. 4). The 48-nt (and 78-nt) cDNAs only detected in cells containing active Xrn1 (Fig. 4c) strongly suggest that the 5'-NGD endonucleolytic products are covered by two and three ribosomes, respectively. The production of cDNAs of exactly the predicted sizes (48 and 78 nts) is an independent confirmation that the 3'-extremity of the 5'-NGD product corresponds precisely to the proposed NGD endonucleolytic cleavage site (Supplementary Fig. 4). Remarkably, the 3'-extremity of the 5'-NGD RNA was detected in the context of active 3'-5' exonucleases, meaning that ribosomes run on and cover the 3'-extremity before any 3'-5' attacks can occur. In summary, we propose that the B4 RNA is produced when associated with three ribosomes and that at least two upstream ribosomes promptly protect the resulting 5'-NGD fragment from degradation (Fig. 4d).

The 5'-OH endocleaved product is phosphorylated by Rlg1/Trl1

Cleaved B4 RNAs were found to be 5'-hydroxylated in *dom34* cell extracts (Fig. 3a). In contrast, we observed that a major portion of B4 RNAs from *dom34*/*xrn1* and *dom34*/*xnr1*/*dxo1* cell extracts can be degraded by Xrn1 *in vitro* without prior 5'–phosphorylation (Supplementary Fig. 1e, 2b), suggesting that B4 accumulates as a 5'-phosphorylated species in this mutant background. We believe that the B4 RNAs in *dom34* mutant cells and *dom34*/*xrn1* mutant cells (i.e in *dom34*/*xrn1*/*dxo1* mutant cells) differ by their association with three and two ribosomes, respectively (Fig. 1e, 1i and Supplementary Fig. 1c, 2b) and hypothesise that the dissociation of the third ribosome post-cleavage gives access to an RNA kinase. A well-characterized factor with RNA kinase activity in yeast is the essential tRNA ligase Trl1, alias Rlg1 (Phizicky *et al*., 1992; Wu and Hopper, 2014). Splicing of tRNAs is known to generate 5'OH-intron RNAs which require Rlg1 kinase activity to permit their degradation by Xrn1. We therefore asked whether the 3'-NGD B4 RNA fragments were substrates of Rlg1. If Rlg1 were required for B4 degradation, loss of Rlg1 function should increase the amount of Dxo1-resistant 5'-OH B4 RNA in *xrn1*/*dom34* cells, where the most of this RNA species has a 5'-monophosphate. Since *RLG1* is an essential gene, we used a temperature sensitive (ts) allele of *RLG1* (*rlg1-4*) for this experiment (Phizicky *et al*. 1992; Wu and Hopper, 2014). RNAs isolated from *rlg1-4*/*xrn1*/*dom34* cells were compared with those from *xrn1*/*dom34* cells by northern analysis (Fig. 5a). After a 2 or 3-hour shift to 37°C, RNAs isolated from *rlg1-4* cells showed a clear accumulation of B4 RNA at the expense of the most abundant B3 species produced by Dxo1 in this genetic background. However, the disappearance of the Dxo1 specific B3 band in favor of an accumulation of B4 in *RLG1+*/*xrn1*/*dom34* mutant cells when shifted from 23°C to 37°C (Fig. 5a) suggested that Dxo1 is naturally thermosensitive, complicating the interpretation of this northern blot (Supplementary Fig. 5a). We therefore did an experiment to show that the accumulation of B4 seen upon thermo-inactivation of the *rlg1-4* allele is due to accumulation of 5'-OH RNAs and not a simple inactivation of Dxo1. We treated total RNA from *rlg1-4*/*dom34*, *xrn1*/*dom34* and *rlg1-4*/*xrn1*/*dom34* with Xrn1 *in vitro* and showed that the accumulation of B4 RNA lacking a 5'-phosphorylated extremity (*i.e*. Xrn1 resistant *in vitro*) at the non-permissive temperature correlated with the presence of the *rlg1-4* ts mutation (Fig. 5b and 5c). We also observed that *rgl1-4* mutants grow for several hours at 37°C, and that 100% of the B4 RNA species lacks a 5'-phosphorylated extremity after a 16-hour shift at

37°C (Supplementary Fig. 5b, 5c). The RNA kinase activity of Rlg1 is thus required for the 5'-exoribonucleolytic digestion of 3'-NGD RNA products.

Identification of NGD cleavage products on mRNAs containing rare codons

We asked whether we could identify endonucleolytic cleavages on another NGD-targeted mRNA, using what we learned about this process on truncated mRNAs. We chose an mRNA containing four contiguous rare CGA codons, which we call $(CGA)_4$-mRNA, as an NGD target (Fig. 6a and Supplementary Fig. 6a) [5]. Similarly to the truncated mRNAs, ribosomes were shown to stall when decoding rare codons and 5'- and 3'-NGD RNAs were produced (Fig. 6a). As previously demonstrated [5,32], we verified that 3'-NGD RNAs fragments can be detected in *dom34* or *DOM34* genetic contexts by northern blotting experiments using probe prB (Supplementary Fig. 6b). The precise identification of endonucleolytic cleavages by primer extension experiments is known to be challenging [5] probably because, in contrast to truncated mRNAs, the positioning of ribosomes on contiguous rare codons is less precise. We first asked whether we could detect the resulting 5'-NGD RNAs (Fig. 6a) using the same procedure as for NGD-targeted truncated RNAs (Fig. 4a and 4b). By probing the $(CGA)_4$-mRNA in a large region upstream of the four CGA codons (Supplementary Fig. 6a), we detected RNA bands using a probe annealing 71 nts upstream of the first rare codon (probe prH, Fig. 6b and Supplementary Fig. 6a). Similar to the 5'-NGD RNAs produced from NGD-targeted mRNA1 (Fig. 4b), RNA detection required *dom34* genetic backgrounds (Fig. 6b). The profile of the 5'-NGD RNAs resulting from endonucleolytic cleavages of $(CGA)_4$-mRNA are remarkably similar to B1, B4 and B5 RNAs from the truncated mRNA1. We then treated these RNAs with Xrn1 and, as anticipated, we showed that the ~71-nt RNAs, like B4 RNAs, are Xrn1-resistant, and that ~47-nt and ~77-nt RNAs, like B1 and B5 RNAs, were Xrn1-sensitive. These results strongly suggest that NGD-targeted $(CGA)_4$-mRNAs are a source of truncated RNAs which are, in turn, processed like mRNA1 by the NGD pathway.

The detection of short RNA species by prH probe suggested that endonucleolytic cleavages occurred just downstream, in a region located ~70 nts upstream of the cluster of rare codons (Supplementary Fig. 6a). We thus set out to map the NGD cleavage sites on the $(CGA)_4$-mRNA, using 3'-RACE for the detection of 5'-NGD RNA 3'-ends in *ski2* and *ski2*/*dom34* mutant cells (Supplementary Fig. 6c). We obtained major RT-PCR products of about 45 bp that were purified, cloned and sequenced (Fig. 6d and Supplementary Fig. 6d). The sequences of the 3'-ends (Fig. 6e) formed three clusters, C1, C2 and C3 (Fig. 6g), that

map to ~71 nts upstream of the second, third and fourth rare codon, respectively, consistent with cleavage within the footprint of the third ribosome as seen for the truncated mRNA1. No 3'-ends were detected within the region covered by the two ribosomes, comforting the notion that disomes are not competent for NGDase activation. Xrn1 arrests mapping to 17-18 nts upstream of the A-site of the two first ribosomes positioned with either the second or third CGA codon in the A-site were also detected through primer extension experiment (Fig. 6f, 6g and 6h). The strongest Xrn1 arrests corresponded to those where the lead ribosome contains the third CGA codon in the A-site (Fig. 6h), suggesting that the major stall occurs on this codon. Typically, Xrn1 is preferentially blocked 17 nts upstream of the first ribosomal A-site residue [23]. We speculate that this 1-nt difference reveals distinct conformations of stalled ribosomes on rare codons versus truncated mRNAs. All these results taken together suggest that the $(CGA)_4$-mRNA and truncated mRNA1 are NGD-targeted in a highly similar process that results in cleavage within the footprint of the third ribosome, 71 nts upstream of the stall site for the leading ribosome.

Discussion

In this study, we first characterized the 3'-NGD RNA fragments produced near the 3'-end of truncated mRNAs that mimic natural cleaved mRNAs known to be NGD targets. One advantage of studying the 3'-NGD products of truncated mRNAs is that the positioning of stalled ribosomes results in 3'-NGD RNA fragments of specific sizes. Using a ribozyme to efficiently generate precise 3'-ends within an open reading frame, we were able to obtain detailed information about the ribosomal positioning on 3'-NGD RNAs, and provide the first precise mapping of the original site of endonucleolytic cleavage on an NGD substrate. Our model suggests that this occurs 8 nts upstream of the first P-site nt of the third ribosome stalled at the 3'-end of the truncated mRNA (Fig. 1i and Fig. 7). This localizes the cleavage within the mRNA exit tunnel, 4 nts before the RNA emerges from the ribosome and becomes available for cleavage by RNase I, classically used in ribosome foot-printing studies. This site is consistent with the idea that the NGD endonuclease, NGDase [19], might be the ribosome itself. However, we cannot fully exclude the possibility the stalled ribosome allows access to an external nuclease with a specific conformation to penetrate this far into the mRNA exit tunnel.

The NGD endonucleolytic cleavage detected within the third stalled ribosome, suggests that the first two stalled ribosomes are not competent for the activation of the NGDase. Here we use the term disome to designate the two first ribosomes blocked in elongation and inactive for RNA cleavage (Fig. 7). The 3'-RACE experiments did not amplify DNA products corresponding to RNAs having the predicted sizes of NGD-cleaved RNAs with the second (41 nts) or first stalled ribosome (15 nts) (predicted sizes 95 and 125 nts), suggesting that they do not occur to any significant level. The major ~65-bp RT-PCR products obtained corresponded perfectly to RNAs cleaved 71nt upstream of the 3'-extremity of mRNA1, suggesting this is the primary site of NGD cleavage.

Xrn1 treatment of various mutant cell extracts suggested that the predominant configuration on truncated mRNAs is disomes. Interestingly, the existence of disomes on truncated mRNAs has been previously reported in ribosome profiling analysis [19] and stacking of two or more ribosomes has recently been proposed as a prerequisite for the activation of the endonuclease [24]. The latter observation led to the proposition that ribosome collision triggers NGDase. We propose another model in which disomes are not competent for NGDase activation, but that three or more ribosomes are required. This suggests that the conformation of disomes is particular and incompatible with NGDase activation. On the contrary, the repetitive band pattern in our northern blot analyses of stalled complexes (Fig. 1c and 4b) suggests that five or more ribosomes are present on the mRNA1 construct and that the third ribosome and those further upstream are all competent for NGD cleavage. The ability to induce NGD cleavage appears thus to be a normal property of stalled ribosomes, with disomes being an exception.

The *dom34* mutation can exaggerate the ribosome stalling and can facilitate the cleavage beyond what would naturally be observed. As discussed in the introduction, analysis of NGD RNA fragments is facilitated by the *dom34* mutation and is crucial for RNA stabilization when analysing truncated mRNAs by northern blotting experiments [5,19]. In the presence of Dom34, and more efficient ribosome dissociation, the exosome would certainly be more actively involved once the first endonucleolytic cleavage event has occurred [5,19]. Importantly, the 3'-RACE experiments confirmed the existence of 5'-NGD products having 3'-ends matching to the 5'-extremity of the 3'-NGD B4 RNA in Dom34 active cells (Fig. 3c and 3d). These observations were used to map endonucleolytic cleavages that occur on a second NGD-target mRNAs containing rare codons, in a *DOM34* genetic context. Endonucleolytic cleavages were mapped 71nts upstream of the first residue in the first ribosome A-site, in the region potentially covered by the third ribosome. We propose that in

this case also, a particular conformation, or associated factor of disomes are responsible for their inability to trigger NGDase activity.

Our experiments also show that NGDase produces downstream cleavage products bearing a 5'-hydroxyl group (Fig. 3a), typical of cleavage reactions not involving a metal ion. We show that the Rlg1/Trl1 kinase, in addition to its role in tRNA splicing, phosphorylates the 3'-NGD fragment to allow degradation by Xrn1 and Dxo1 (Fig. 5 and Supplementary Fig. 5). The resistance of the 3'-NGD B4 RNA fragments to Xrn1 attacks *in vitro* and *in vitro* (Fig. 1e) is likely to be a direct consequence of the presence of the third ribosome preventing access to Rlg1/Trl1. Accordingly, extremities of the B4 RNAs were shown to be predominantly 5'-hydroxylated in a *dom34* context, while an important portion of B4 RNAs are 5'-monophosphorylated in *dom34*/*xrn1* and *dom34*/*xrn1*/*dxo1* mutant cell extracts, where these RNAs accumulate in the absence of Xrn1 and are mostly associated with disomes. Rlg1 is thus a far more general RNA kinase than previously suspected, and also acts in the NGD pathway.

The unexpected function of Dxo1 in the NGD pathway might appear secondary but its implication can explain the heterogeneity of 3'-NGD RNA fragments observed in *xrn1 or xrn1*/*dom34* mutant cells. Xrn1 and Dxo1 activities, combined with Rlg1/Trl1 RNA kinase activity have likely masked the detection of the major NGD cleavage products in previous studies. Additionally, the fact that we observed that the 5'-3' exoribonucleolytic activity of Dxo1 is naturally thermosensitive raises the question of its known decapping activity on unmethylated-capped mRNAs and the biological consequences of their accumulation at high temperature [25].

In conclusion, NGDase cleavage does not randomly occur upstream of the ribosomal stall and is not an artefact of *dom34* genetic context. It can also be precisely mapped as a unique cleavage event within the ribosomal mRNA exit tunnel at 8 nt of the P-site residue. Remarkably, mRNAs containing rare codons are processed similarly, but cleavage accuracy is slightly affected and might be explained by a particular conformation of the first stalled ribosomes that correlates with specific Xrn1 arrests (Fig. 6f). Ribosomal A-site and occupancy of the mRNA entrance tunnel by mRNAs containing rare codons could explain some of the minor differences observed with truncated mRNAs. We also learned that 5'-OH NGD RNA fragments are produced, phosphorylated by Rlg1/Trl1 and degraded by Xrn1 and alternatively by Dxo1. Indeed, we learned that the inactivation of Xrn1 can lead to a Dxo1 trimming that can mask many original cleavages and can scramble global analysis. Moreover,

Rlg1-Xrn1-(Dxo1) may potentially play a general role in the healing and degradation of a multitude of other 5'-hydroxylated RNAs, such as those identified by Peach *et al*. [33]. It will be also interesting to confirm a role of all these factors for these substrates in yeast and for its homologous kinase hClp1 in human cells [34]. In conclusion, this study provides very important new mechanistic insights that will help to go further in the comprehension of all mRNA surveillance pathways in connection to NGD.

Figure 1

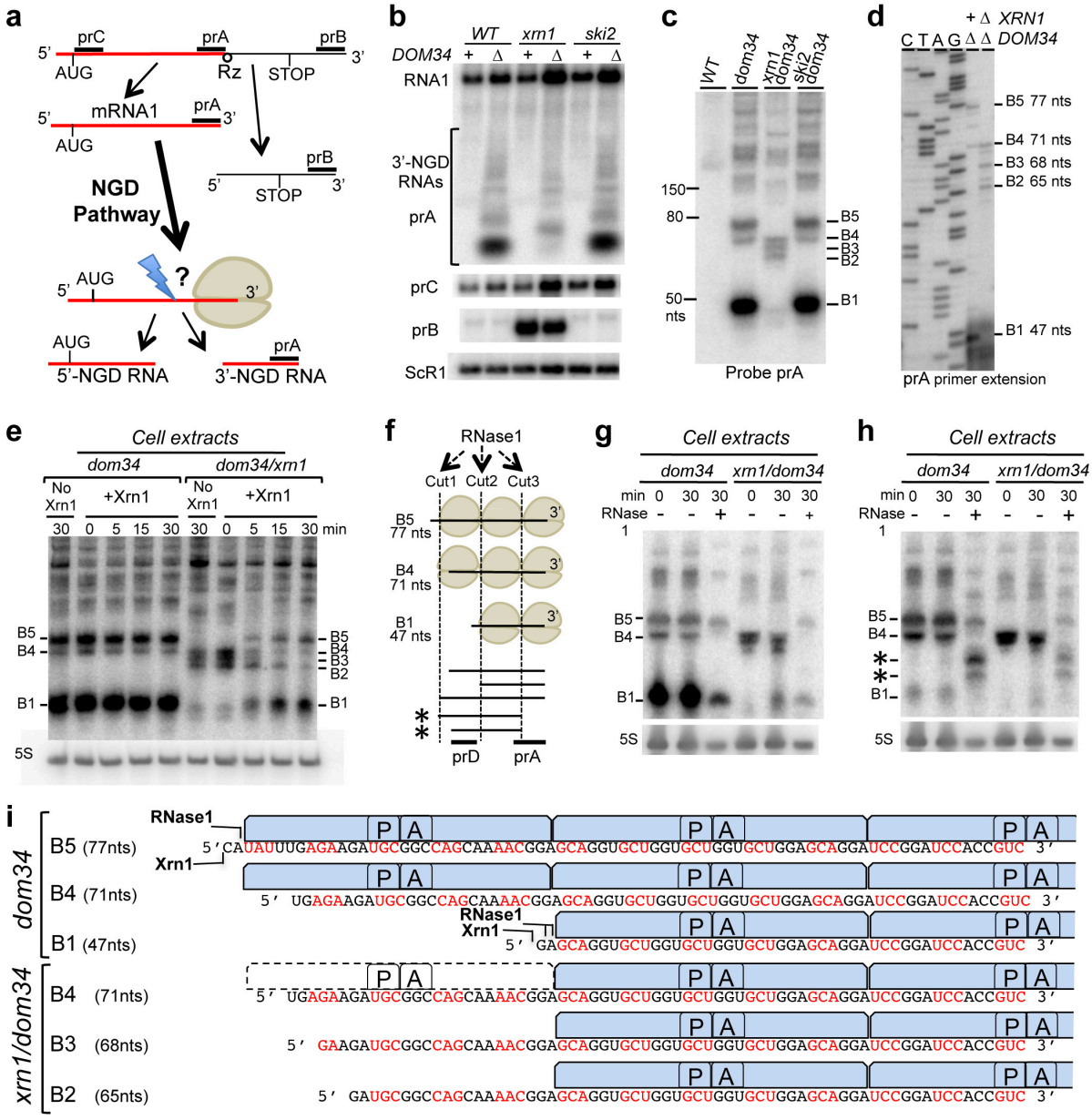

Fig.1: Size characterization of 3'-NGD RNA fragments at single nucleotide resolution and **RNase ribosomal protection assay (a)** Schematic view of the URA3Rz mRNA showing the ribozyme (Rz) site (see detailed sequence in Supplementary Fig. 1a). Translational start (AUG) and stop codons are indicated. RNA1 (in red) is the truncated stop-less codon mRNA following ribozyme cleavage (see also Supplementary Fig. 1a). Probes prA, prB and prC used in northern blots analysis are indicated. 5' and 3'-NGD RNAs are the resulting products of NGD cleavage of mRNA1. The lightning flash represents the NGD endonucleolytic cleavage upstream of the ribosome stall site and probe prA is designed for the detection of all potential 3'-NGD RNAs (see also Supplementary Fig. 1a) **(b)** Agarose gel followed by northern blot

showing steady state levels of RNA (RNA1 and 3'-NGD RNA fragments) in wild-type and the indicated mutant strains. The scR1 RNA served as a loading control **(c)** 8% PAGE followed by northern blot analysis using probe prA showing steady state levels of 3'-NGD RNA in the indicated mutant strains **(d)** Primer extension experiments using probe prA to determine the 5'-end of 3'-NGD RNAs. B1, B2, B3, B4 and B5 RNAs shown in Fig. 1c are indicated with the corresponding size calculated by primer extension. (**e**) Xrn1 treatment *in vitro* of cell extracts (*i.e*. mRNAs in presence of ribosomes) from *dom34* or mutant cells, followed by RNA extraction and northern blot using probe prA. Sizes in nts are deduced from experiments (**c**) and (**d**). (**f**) Schematic view of ribosomes covering RNA species B1, B4 and B5 observed in *dom34* mutant cells. Cut1, Cut2 and Cut3 represent potential RNase I cleavage sites. Probes prA, and prD used in northern blots analysis shown in (**g**) and (**h**) are indicated. 5'-extremities of B5 and B4 RNAs potentially protected by two ribosomes and detected by prD are indicated by asterisks. (**g**) RNase I treatment of cell extracts *in vitro*, analysed as in (**e**). (**h**) Membrane in (**g**) has been probed with prA. (**i**) Schematic view of the ribosome positioning on 3'-NGD RNAs combining information about single-nucleotide size resolution, ribosomal association, and Xrn1 or RNase I ribosomal protection of 3'-NGD RNAs. ORF codons are shown in black or red. A and P are ribosomal A- and P-sites respectively.

Figure 2

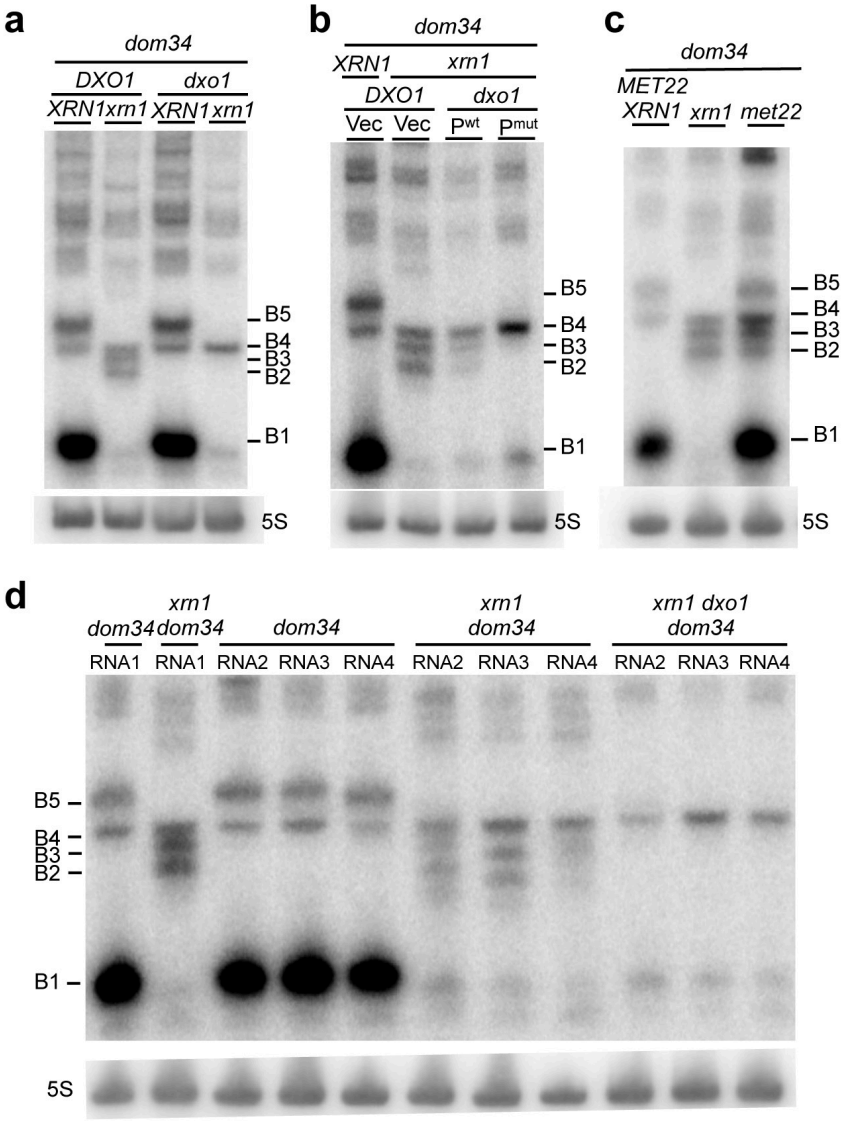

Fig. 2: Dxo1 creates the heterogeneity of 3'-NGD RNA fragments in Xrn1 deficient cells. 8% PAGE followed by northern blot analysis using probe prA showing steady state levels of RNAs in *dom34* and other indicated mutant strains. The 5S rRNA served as a loading control **(a)** Impact of *DXO1* deletion on B2 and B3 RNA production. (**b**) Plasmid expression of wild-type Dxo1 (P^{wt}) or a Dxo1 catalytic mutant (P^{mut}) (mutant E260A/D262A) [25]. The vector control is plasmid pRS313 (Vec). (**c**) Detection of B2 and B3 RNAs under conditions of partial Xrn1 inhibition in *met22* mutant strain. (**d**) Dxo1-dependent production of 3'-NGD RNAs in the context of RNA2, RNA3 and RNA4, whose 5'-sequences differ from that of the RNA1 3'-NGD (see Supplementary Fig. 2d).

Figure 3

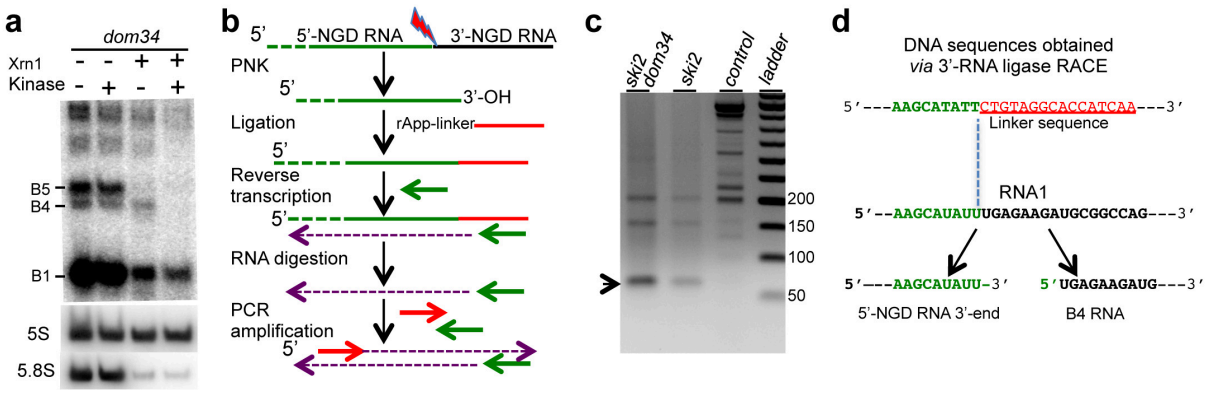

Fig. 3: Characterization of the endonucleolytic RNA fragments. (**a**) Xrn1 digestion of total RNA extracts from *dom34* mutant cells in the presence or absence of T4 polynucleotide kinase *in vitro*. 8% PAGE followed by northern blot analysis using probe prA. The 5S rRNA served as a loading control and 5.8S rRNA as a positive control of Xrn1 treatment (**b**) Flow chart illustrating the method used for 3'-end mapping, called 3'-RNA ligase mediated RACE as described in [31] with minor modifications according to [30] (see experimental procedures). (**c**) PCR products obtained from 3'-RACE and migrated on 2% agarose gel. Purified DNAs for sequencing are indicated by an arrowhead. Prior to PCR, cDNAs were produced from total RNA from *ski2*, *ski2*/*dom34* mutant cells expressing RNA1. Control is made of total RNA from *ski2*/*dom34* mutant cells without RNA1 expression. (**d**) Sequences obtained after 3'-RACE performed on *ski2* and *ski2*/*dom34* total RNA. 100% of sequenced clones (omitting a residual 5S rRNA-linker amplification detected) have this DNA sequence. 5'-NGD DNA sequence (in green) and linker sequence (in red). Below, the site of RNA1 is shown before and after the cleavage producing the 3'-NGD RNA B4 and the 3'-extremity of the 5'-NGD RNA confirmed by 3'-RACE.

Figure 4

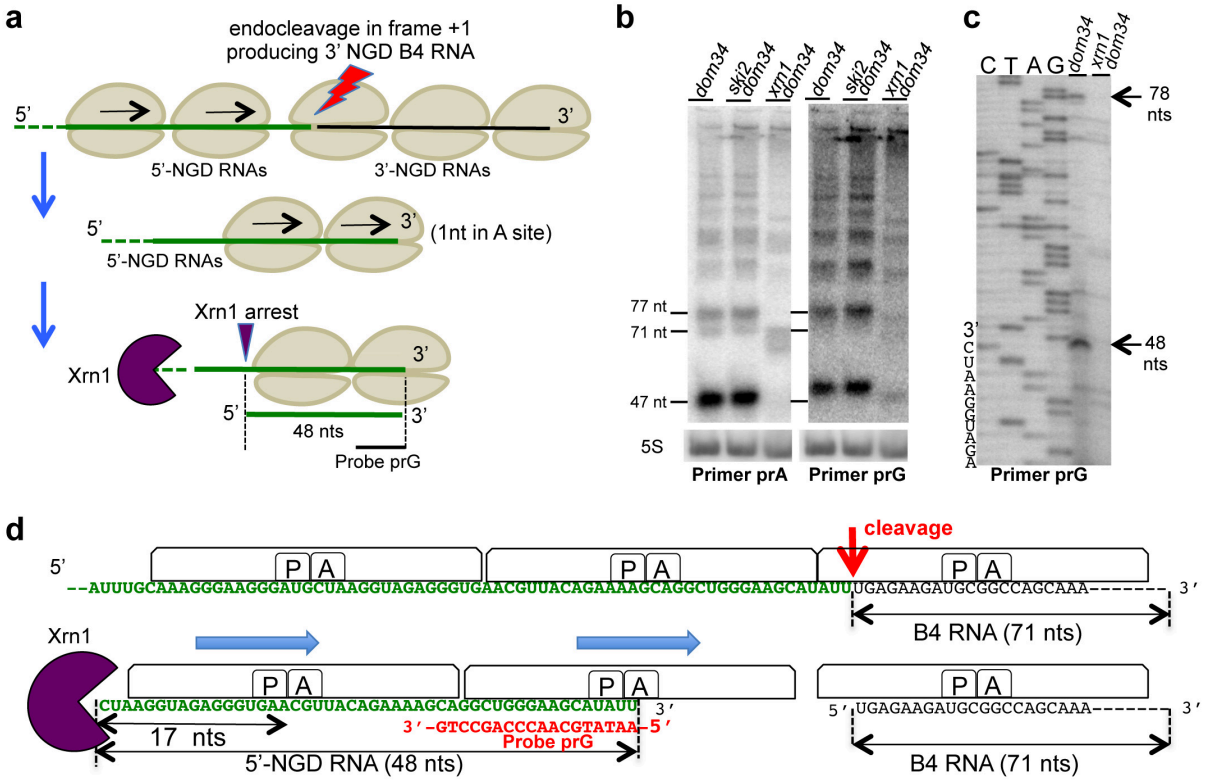

Fig. 4: Analysis of the fate of 5'-NGD RNAs. (**a**) Schematic model of RNA1 before and after the endonucleolytic cleavages producing B4 RNAs. 5'-NGD resulting RNAs are shown here covered by two ribosomes and processed by Xrn1 to 48-nt RNAs (see also Supplementary Fig. 4 for 5'-NGD RNAs covered by three ribosomes). (**b**) 8% PAGE followed by northern blot analysis using probe prG showing steady state levels of RNAs in the indicated mutant strains (left panel). Same membrane has been probed with prA as a ladder (right panel), and sizes of B5 (77nt), B4 (71 nt) and B1 (47nt) are indicated. The 5S rRNA served as a loading control. **(c)** Primer extension experiments using probe prG to determine the 5'-end of RNAs (see also Supplementary Fig. 5). (**d**) Schematic model of ribosome positioning on RNA1 before and after the unique endonucleolytic cleavage producing B4 RNAs, localized 8 nts upstream of the first P-site nt. The position of disomes on the resulting 48-nt 5'-NGD RNA is shown with the distal ribosome having 1 nt in the A site (see also Supplementary Fig. 4).

Figure 5

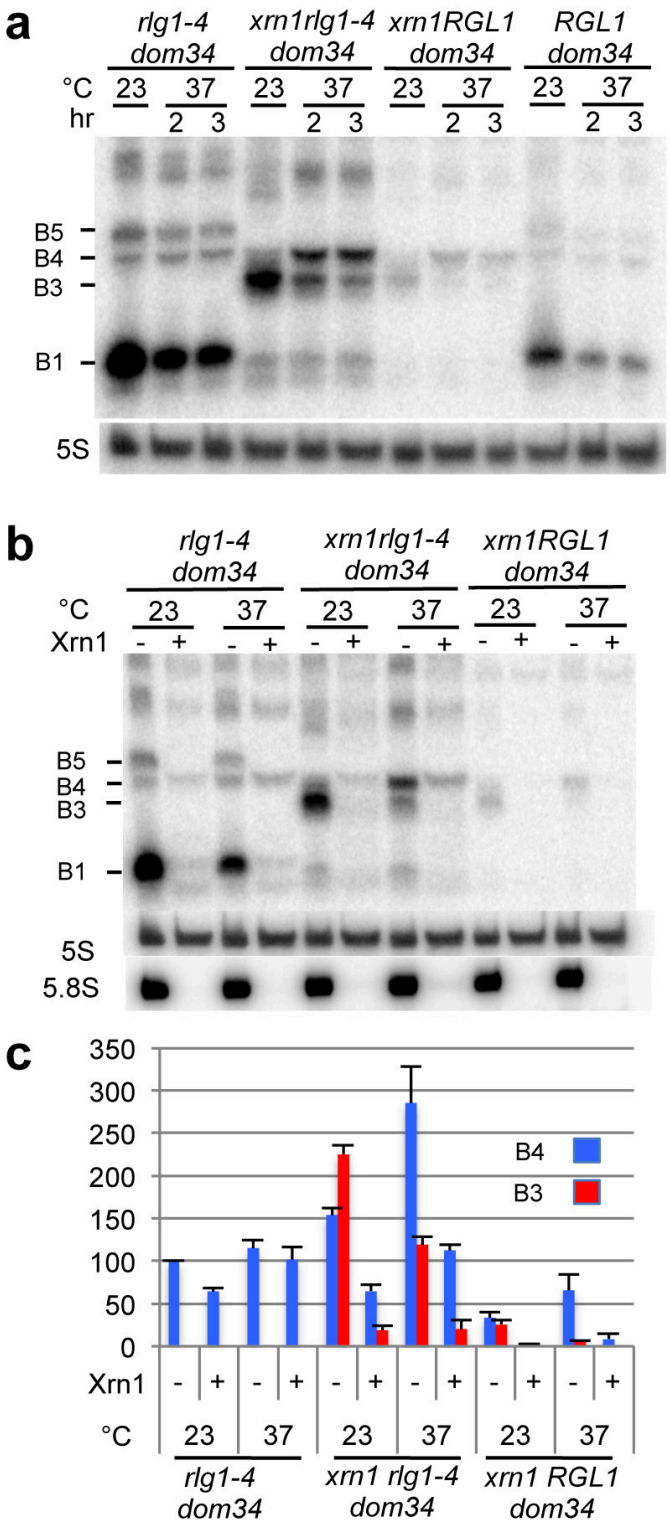

Fig. 5: Endonucleolytically cleaved 5'-OH RNAs are phosphorylated by Rlg1/Trl1. (**a**) 8% PAGE followed by northern blot analysis using probe prA. Levels of 3'-NGD RNA fragments in *rlg1-4* and other indicated mutant strains cells at 23°C and after a shift to the non-permissive temperature (37°C) for 2 or 3 hours. (**b**) Xrn1 treatment *in vitro* of total RNA from *rlg1-4* and other indicated mutant strains grown at 23°C or after a 3h shift at 37°C as described in (**a**). The 5S rRNA served as a loading control and 5.8S rRNA is a positive control of Xrn1 treatment. (**c**) From experiments shown in (**b**), B3 and B4 RNA quantifications were standardized using 5S rRNA. Levels of RNAs were plotted as a % of B4 RNA amount in *rlg1-4/dom34* cells at 23°C. All quantifications are indicated with standard errors calculated from three independent experiments.

Figure 6

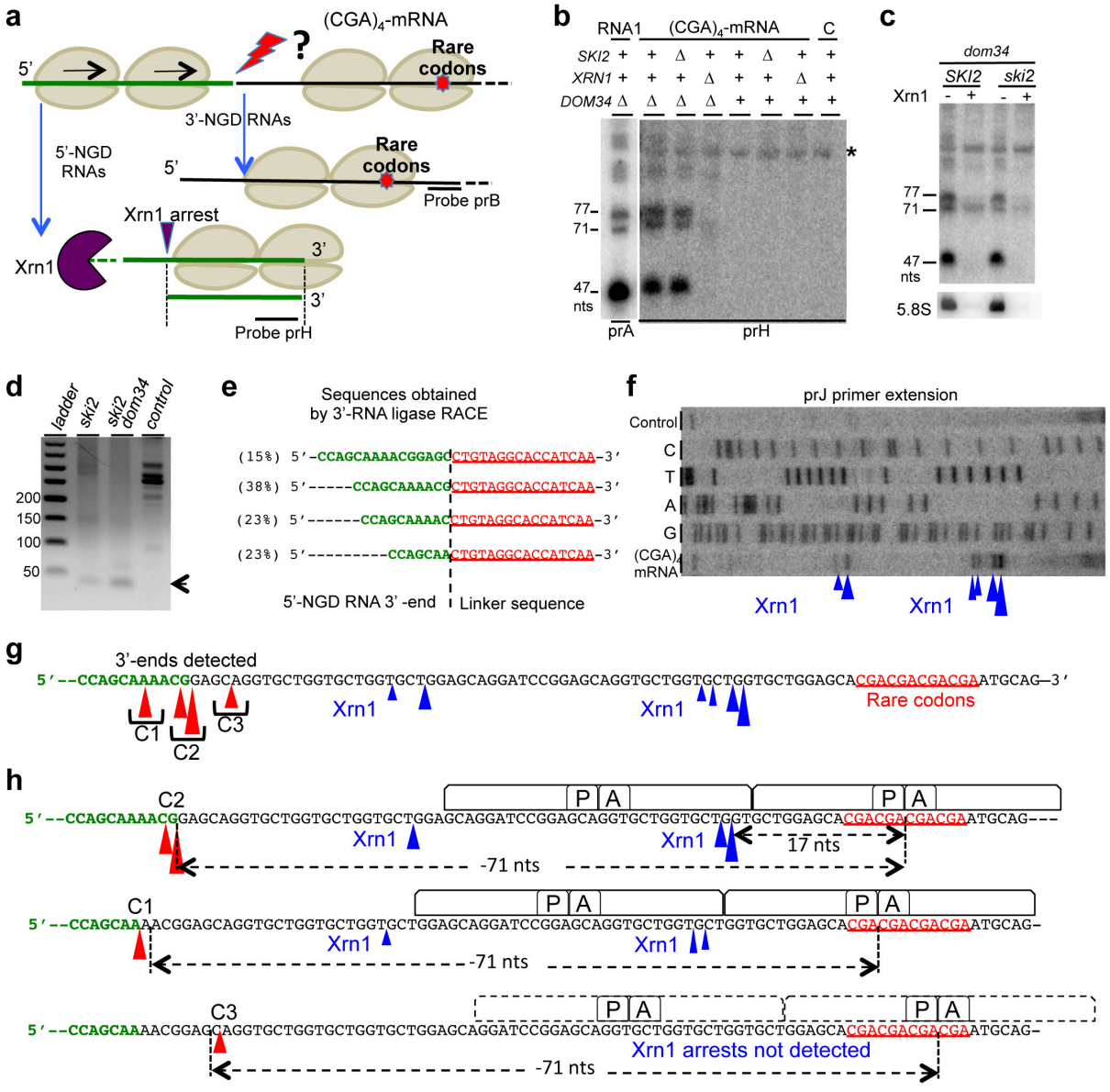

Fig. 6: identification of the endonucleolytic cleavages on the NGD targeted $(CGA)_4$-mRNA. (a) Schematic view of the $(CGA)_4$-mRNA. 5'- and 3'-NGD RNAs are the expected products of NGD. The lightning flash represents the potential endonucleolytic cleavage upstream of the ribosome stall site. Probes prB and prH are indicated. 5'-NDG RNAs are shown potentially processed by Xrn1 as described in Fig. 4 and Supplementary Fig. 4. **(b)** 8% PAGE followed by northern blot analysis using probe prH showing steady state levels of

RNAs in the indicated mutant strains. Same membrane has been probed with prA as a ladder, and sizes of RNA1 products such as B5 (77nt), B4 (71 nt) and B1 (47nt) are indicated. Only the *dom34* lane is shown. See Supplementary Fig. 6a for the sequence probed by prH. The 5S rRNA served as a loading control. Total RNA from WT cells without $(CGA)_4$-mRNA expression served as a control, noted C. A non-specific band is indicated by an asterisk. (**c**) Xrn1 treatment *in vitro* of total RNA from *dom34* or *dom34*/*ski2* mutant cells and northern blot using probe prH. The 5.8S rRNA is a positive control of Xrn1 treatment **(d)** PCR products obtained from 3'-RNA ligase mediated RACE (see also Fig. 3c). Prior to PCR, cDNAs were produced from cells expressing $(CGA)_4$-mRNA. Total RNA from cells without $(CGA)_4$-mRNA expression served as a control. (**e**) Sequences obtained after 3'-RACE performed in (d) on *ski2*/*DOM34* total RNA. Sequence distribution is given in percentage. (**f**) Primer extension experiments using probe prJ to determine the 5'-end of RNAs. Xrn1-specific arrests are indicated by arrowheads. (**g**) Positioning of 3'-ends detected by 3'-RACE on $(CGA)_4$-mRNA from *ski2*/*DOM34* cells (red arrowhead). Arrowhead sizes are proportional to the relative number of sequences obtained. Three cleavage clusters, C1, C2 and C3 were defined (see also Supplementary Fig. 6d). Xrn1 arrests deduced from primer extension (**f**) are indicated by black arrowhead with sizes proportional to the intensity of reverse stops observed in (**f**). (**h**) Schematic view of the ribosome positioning on $(CGA)_4$-mRNA deduced from Xrn1 arrests combined with the positioning of endonucleolytic cleavages provided by 3'-RACE.

Figure 7

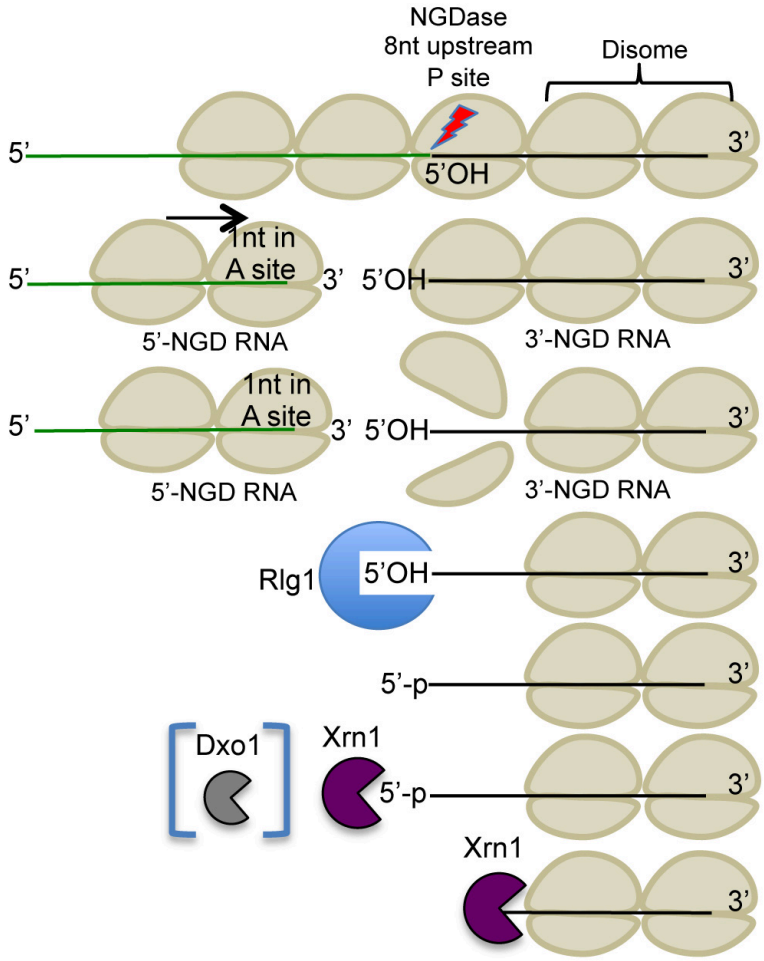

Fig. 7: Model of No-Go decay pathway involving NGDase cleavage within ribosomal mRNA exit tunnel, RNA kinase Rlg1/Trl1 and 5'-3' exoribonucleases. Here, the third ribosome is represented as competent for NGDase activation, but upstream ribosomes are also competent. We propose that the two first stalled ribosomes are not properly conformed to trigger the endonucleolytic process. NGDase cleavage (lightning flash) occurs 8 nts upstream of the first P-site residue, within the mRNA exit tunnel of the ribosome. Upstream ribosomes covering the resulting 5'-NGD fragments can advance and stall on the new 3'-end with 1 nt in the ribosomal A-site. After endonucleolytic cleavage, the NGD-competent ribosome dissociates and facilitates access of the RNA kinase Rlg1/Trl1 to the 5'-hydroxylated 3'-NGD RNA. Once the RNA is 5'-phosphorylated, the processive 5'-3' exonucleolytic activity of Xrn1 can degrade, or alternatively, 5'-3' exonucleolytic digestion of this RNA by Dxo1 can occur.

METHODS

Yeast Media, plasmids, strains, and oligonucleotides. The media, plasmids, strains of *S. cerevisiae,* and oligonucleotides used in this study are described in supplemental information.

Northern blot analysis. RNA Extracts and northern blots were performed as described previously (Sinturel *et al*., 2012). Total RNA was resolved by 8% TBE-Urea polyacrylamide or 1.4%TBE-Agarose gels. Blots were exposed to PhosphorImager screens, scanned using a Typhoon FLA 9500 (Fuji), and quantified with ImageJ software.

***In vitro* RNA digestion.** 5µg of total RNA or $2OD_{260nm}$ of cell extracts were digested by 1 unit of Xrn1 (Biolabs) in NEB buffer 3 at 25°C during 30 min unless otherwise indicated. NEB Buffer 3 was replaced by Kinase NEB buffer in all kinase assays in the presence or absence of Xrn1 (Fig. 5a). For RNase I treatment of cell extracts, $2OD_{260nm}$ of extracts (prepared without heparin) were incubated with 0.5 µl, 1 µl and 2 µl RNase I (Invitrogen, 100 units/ml) 30 min at 25°C. For total RNA treatment, 5µg of RNA were digested by 0.5 µl of RNase I, 30 min at 25°C. All RNase treatments were followed by RNA extraction and northern blot analysis as described above.

Primer Extension. Radiolabeled primers (primers prA and prE for RNA1, and primer prJ for for $(CGA)_4$-mRNA) were used and reverse transcriptase (ThermoFisher) was used to synthesize a single-stranded DNA toward the 5'-end of the RNA. The size of the labeled single-stranded DNA was determined relative to a sequencing ladder (ThermoFischer Sequenase sequencing kit) on 5% TBE-Urea polyacrylamide gel. Oligonucleotides were radio-labeled with [γ -32P]ATP with the T4 polynucleotide kinase (Biolabs).

3'-end RNA mapping. Mapping was performed according to the 3'-RNA ligase mediated RACE method described previously [31] with minor modifications: Total RNA preparations were first 3'-dephosphorylated using T4 PNK 1h at 37°C without ATP and pre-adenylated linker (Universal miRNA cloning linker, NEB) ligation was performed during 4h at 22°C in the presence of truncated ligase 2 (NEB) [30]. Reverse transcriptase reactions were performed using reverse primer prE complementary to the linker sequence. PCR primer prF specific to RNA1, or primer prK specific to $(CGA)_4$-mRNA, were used with primer prE in PCR

reactions (Supplementary Fig. 3a and 6c). PCR products were purified, cloned into zero Blunt TOPO PCR Cloning vector (Invitrogen), transformed and plasmids sequenced.

REFERENCES

1 Doma, M. K. & Parker, R. Endonucleolytic cleavage of eukaryotic mRNAs with stalls in translation elongation. *Nature* **440**, 561-564, (2006).

2 Passos, D. O. *et al.* Analysis of Dom34 and its function in no-go decay. *Mol Biol Cell* **20**, 3025-3032, (2009).

3 Chen, L. *et al.* Structure of the Dom34-Hbs1 complex and implications for no-go decay. *Nat Struct Mol Biol* **17**, 1233-1240, (2010).

4 Letzring, D. P., Dean, K. M. & Grayhack, E. J. Control of translation efficiency in yeast by codon-anticodon interactions. *RNA* **16**, 2516-2528, (2010).

5 Tsuboi, T. *et al.* Dom34:hbs1 plays a general role in quality-control systems by dissociation of a stalled ribosome at the 3' end of aberrant mRNA. *Mol Cell* **46**, (2012).

6 Simms, C. L., Hudson, B. H., Mosior, J. W., Rangwala, A. S. & Zaher, H. S. An active role for the ribosome in determining the fate of oxidized mRNA. *Cell reports* **9**, 1256-1264, (2014).

7 Sinturel, F. *et al.* Cytoplasmic Control of Sense-Antisense mRNA Pairs. *Cell reports* **12**, 1853-1864, (2015).

8 Simms, C. L., Thomas, E. N. & Zaher, H. S. Ribosome-based quality control of mRNA and nascent peptides. *Wiley interdisciplinary reviews. RNA* **8**, (2017).

9 Guydosh, N. R. & Green, R. Translation of poly(A) tails leads to precise mRNA cleavage. *Rna* **23**, 749-761, (2017).

10 Frischmeyer, P. A. *et al.* An mRNA surveillance mechanism that eliminates transcripts lacking termination codons. *Science* **295**, 2258-2261 (2002).

11 van Hoof, A., Frischmeyer, P. A., Dietz, H. C. & Parker, R. Exosome-mediated recognition and degradation of mRNAs lacking a termination codon. *Science* **295**, 2262-2264. (2002).

12 Kuroha, K. *et al.* Receptor for activated C kinase 1 stimulates nascent polypeptide-dependent translation arrest. *EMBO Rep* **11**, 956-961, (2010).

13 Brandman, O. *et al.* A ribosome-bound quality control complex triggers degradation of nascent peptides and signals translation stress. *Cell* **151**, 1042-1054, (2012).

14 Defenouillere, Q. *et al.* Cdc48-associated complex bound to 60S particles is required for the clearance of aberrant translation products. *Proc Natl Acad Sci U S A* **110**, 5046-5051, (2013).

15 Shen, P. S. *et al.* Protein synthesis. Rqc2p and 60S ribosomal subunits mediate mRNA-independent elongation of nascent chains. *Science* **347**, 75-78, (2015).

16 Johnson, A. W. & Kolodner, R. D. Synthetic lethality of sep1 (xrn1) ski2 and sep1 (xrn1) ski3 mutants of Saccharomyces cerevisiae is independent of killer virus and suggests a general role for these genes in translation control. *Mol Cell Biol* **15**, 2719-2727 (1995).

17 Shoemaker, C. J., Eyler, D. E. & Green, R. Dom34:Hbs1 promotes subunit dissociation and peptidyl-tRNA drop-off to initiate no-go decay. *Science* **330**, 369-372, (2010).

18 Guydosh, N. R., Kimmig, P., Walter, P. & Green, R. Regulated Ire1-dependent mRNA decay requires no-go mRNA degradation to maintain endoplasmic reticulum homeostasis in S. pombe. *eLife* **6**, doi:10.7554/eLife.29216 (2017).

19 Guydosh, N. R. & Green, R. Dom34 rescues ribosomes in 3' untranslated regions. *Cell* **156**, 950-962, (2014).

20 Eckner, R., Ellmeier, W. & Birnstiel, M. L. Mature mRNA 3' end formation stimulates RNA export from the nucleus. *The EMBO journal* **10**, 3513-3522 (1991).

21 Parker, R. RNA degradation in Saccharomyces cerevisae. *Genetics* **191**, 671-702, (2012).

22 Ingolia, N. T., Ghaemmaghami, S., Newman, J. R. & Weissman, J. S. Genome-wide analysis in vivo of translation with nucleotide resolution using ribosome profiling. *Science* **324**, 218-223, (2009).

23 Pelechano, V., Wei, W. & Steinmetz, L. M. Widespread Co-translational RNA Decay Reveals Ribosome Dynamics. *Cell* **161**, 1400-1412, (2015).

24 Simms, C. L., Yan, L. L. & Zaher, H. S. Ribosome Collision Is Critical for Quality Control during No-Go Decay. *Mol Cell* **68**, 361-373, (2017).

25 Chang, J. H. *et al.* Dxo1 is a new type of eukaryotic enzyme with both decapping and 5'-3' exoribonuclease activity. *Nat Struct Mol Biol* **19**, 1011-1017, (2012).

26 Dichtl, B., Stevens, A. & Tollervey, D. Lithium toxicity in yeast is due to the inhibition of RNA processing enzymes. *The EMBO journal* **16**, 7184-7195 (1997).

27 Todeschini, A. L., Condon, C. & Benard, L. Sodium-induced GCN4 expression controls the accumulation of the 5' to 3' RNA degradation inhibitor, 3'-phosphoadenosine 5'-phosphate. *J Biol Chem* **281**, 3276-3282 (2006).

28 Nagarajan, V. K., Jones, C. I., Newbury, S. F. & Green, P. J. XRN 5'-->3' exoribonucleases: structure, mechanisms and functions. *Biochim Biophys Acta* **1829**, 590-603, (2013).

29 Gonzalez, T. N., Sidrauski, C., Dorfler, S. & Walter, P. Mechanism of non-spliceosomal mRNA splicing in the unfolded protein response pathway. *The EMBO journal* **18**, 3119-3132, (1999).

30 McGlincy, N. J. & Ingolia, N. T. Transcriptome-wide measurement of translation by ribosome profiling. *Methods* **126**, 112-129, (2017).

31 Adkar-Purushothama, C. R., Bru, P. & Perreault, J. P. 3' RNA ligase mediated rapid amplification of cDNA ends for validating viroid induced cleavage at the 3' extremity of the host mRNA. *Journal of virological methods* **250**, 29-33, doi:10.1016/j.jviromet.2017.09.023 (2017).

32 Chen, H. & Xiong, L. The bifunctional abiotic stress signalling regulator and endogenous RNA silencing suppressor FIERY1 is required for lateral root formation. *Plant Cell Environ* **33**, 2180-2190, (2010).

33 Peach, S. E., York, K. & Hesselberth, J. R. Global analysis of RNA cleavage by 5'-hydroxyl RNA sequencing. *Nucleic Acids Res* **43**, (2015).

34 Weitzer, S. & Martinez, J. The human RNA kinase hClp1 is active on 3' transfer RNA exons and short interfering RNAs. *Nature* **447**, 222-226, (2007).

35 Mumberg, D., Muller, R. & Funk, M. Yeast vectors for the controlled expression of heterologous proteins in different genetic backgrounds. *Gene* **156**, 119-122 (1995).

Author contributions:

A.N., S.C., R.S.F., J.H., C.T. and L.B. designed, performed and analysed data. L.B. wrote the manuscript.

Acknowledgements

This work has been supported by AAP Emergence Sorbonne Université, SU-16-R-EMR-03 and by the "Initiative d'Excellence" program from the French State grant "DYNAMO", ANR-11-LABX-0011-01. S.C. was a recipient of fellowship from the Ministère pour la Recherche et la Technologie (MNRT). A.N. was supported by a doctoral grant from "DYNAMO", ANR-11-LABX-0011-01. We thank Eric Phizicky and Anita Hopper for providing *rgl1-4* mutant and derivative strains. We thank Ciaran Condon, Josette Banroques and Kyle Tanner for technical assistance. We thank Ciaran Condon for comments on the manuscript and constructive discussions.

Competing financial interests statement.

The authors declare no competing financial interests.

End notes:

Additional Information: this manuscript contains Supplementary Information, 6 Supplementary Figures and 4 Supplementary Tables.